ISSN:2790-1688 Volume-14-(2025)

Robust Performance Tracking Control for Vehicles Based on Sliding Mode

Yuheng Wu

School of Mechanical and Electrical Engineering, Wenzhou University, Wenzhou, China.

2077319818@qq.com

Abstract. To solve the parameter uncertainty and external disturbance in vehicle trajectory tracking control, this paper proposes a cooperative control architecture based on predictive performance function (PPF) and terminal sliding mode control (TSMC). By constructing a time-varying performance function, dynamically constraining the transient and steady-state performance of the tracking error, and combining the finite-time convergence characteristics of the non-singular terminal sliding surface, this method realizes the global robust adjustment of the tracking error within the preset performance boundary. Lyapunov theory proves the finite-time stability of the closed-loop system and verifies the effectiveness of the cooperative mechanism between PPF and TSMC in suppressing parameter perturbation and external disturbance. According to Simulink simulation results, compared with traditional TSMC and preset performance control strategies, the method proposed in this paper manifests better tracking accuracy and dynamic robustness, which provides the theoretical basis and engineering references for trajectory tracking control of intelligent vehicles in complex environments.

Keywords: Predictive Performance Control, Terminal Sliding Mode Technology, Robustness.

1. Introduction

Vehicle dynamics control is one of the key technologies to realize intelligent driving. However, against complex working conditions such as high-speed cornering and emergency obstacle avoidance, the robustness of existing control strategies encounters severe challenges. Perturbation of model parameters and external interference can easily trigger vehicle yaw instability, decrease trajectory tracking accuracy, and even cause safety accidents. This study aims to overcome the above limitations and explore a new robust tracking control architecture to improve the active safety of intelligent vehicles under extreme working conditions. This research is of great significance to promote the application of intelligent driving technology in practical scenarios.

To tackle the uncertainty in vehicle dynamics control, methods such as sliding mode control (SMC) [1] and model predictive control (MPC) [2] are widely used. However, the dynamic response lag inherent in the approach phase of SMC limits its performance. Although MPC enables multi-objective optimization, its dependence on model accuracy is too high, making it challenging in practical applications. TSMC [3-8] can theoretically achieve finite-time convergence by introducing nonlinear sliding manifolds, but the design of existing TSMC performance functions fails to fully consider the time-varying dynamic characteristics of vehicle systems. In addition, traditional PPC [9-10] usually adopts fixed boundary constraints, which makes it hard to adapt to strict requirements of transient response under sudden working conditions.

To overcome the traditional control limitations in vehicle dynamics control, this study proposes a composite control strategy based on the fusion of PPF [11] and TSMC. Its innovations are mainly as follows. (1) A dynamic PPF with feedforward compensation is proposed, which can adjust the performance boundary constraints based on the real-time prediction of vehicle state evolution trend in an adaptive manner, so as to optimize the transient response of the system. (2) A new non-singular terminal sliding mode surface is designed. Combined with a disturbance observer, the online estimation and compensation of compound disturbance are realized, which significantly improves the system robustness. (3) Compared with traditional TSMC, this control strategy can suppress control chattering and improve control quality while ensuring finite time convergence. Simulink simulation

results verify the effectiveness of the proposed scheme, which indicates that it can largely reduce the yaw rate tracking error and lateral velocity deviation.

2. Problem Description

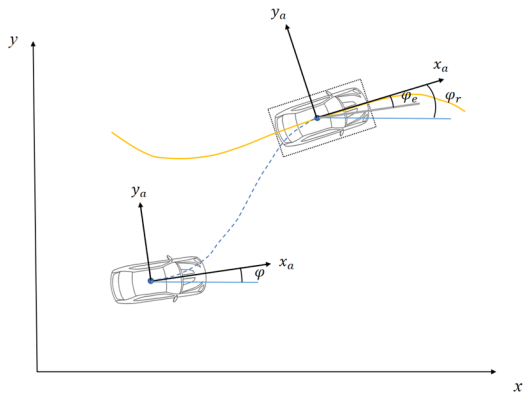

Figure 1 Position Error Relationship Between Actual Vehicle and Reference Vehicle

The motion trajectory of the vehicle in inertial coordinates is shown in Figure 1. The tracking error under fixed coordinates of the vehicle can be expressed as:

$$\begin{bmatrix} x_e \\ y_e \\ \varphi_e \end{bmatrix} = \begin{bmatrix} cos\varphi & sin\varphi & 0 \\ -sin\varphi & cos\varphi & 0 \\ 0 & 0 & 1 \end{bmatrix} \begin{bmatrix} x_r - x \\ y_r - y \\ \varphi_r - \varphi \end{bmatrix} \tag{1}$$

Where x_e , y_e , φ_e are longitudinal error, lateral error and angular error, respectively. (x_r, y_r, φ_r) and $(x, y, \varphi)$are the reference position and actual position of the vehicle in inertial coordinates, respectively. In addition, their differential forms with respect to time are expressed as follows:

$$\begin{cases} \dot{x}_{(r)} = v_{(r)} cos\varphi_{(r)} \\ \dot{y}_{(r)} = v_{(r)} sin\varphi_{(r)} \\ \dot{\varphi}_{(r)} = \omega_{(r)} \end{cases} \tag{2}$$

Where x and $x_{(r)}$ are the actual and reference longitudinal displacements. y and $y_{(r)}$ are actual and reference lateral displacements. φ and $\varphi_{(r)}$ are the actual heading angle and reference heading angle, respectively. Together with (2), (1) is differentiated with respect to time to obtain the following formula:

$$\begin{cases} \dot{x}_e = \omega y_e - v + v_r cos\varphi_e \\ \dot{y}_e = -\omega x_e + v_r + v_r sin\varphi_e \\ \dot{\varphi}_e = \omega_r - \omega \end{cases} \tag{3}$$

Where v_r and ω_r are reference forward speed and the reference yaw rate, respectively. v and ω are the actual speed rate and the actual yaw rate. Thus, the control can be transformed into the design of the speed control law, that is, finding a control signal of the following form:

$$v = v^*(x, y, \varphi, t), \ \omega = \omega^*(x, y, \varphi, t) \tag{4}$$

When t→ +∞ with following restrictions guaranteed simultaneously:

$$|v_{(t)}| \le v_{max}, \omega_{(t)} \le \omega_{max} \quad \forall t \ge 0 \tag{5}$$

To achieve $x_{(t)} \to x_{r(t)}, y_{(t)} \to y_{r(t)}$, $\varphi_{(t)} \to \varphi_{r(t)}$, where v_{max} and ω_{max} are given normal number. These control signals are exactly what is needed in the next stage. Their definition in this study is the speed planning module, which is correspondingly regarded as the speed tracking module in the next stage.

Regardless of the behavior characteristics of the vehicle in rolling, pitching and vertical directions, their dynamic characteristics in the lateral, longitudinal and yaw planes can be studied, which is described by the following formulas:

$$\begin{cases} \dot{v}_x = \frac{F_X - C_a {v_x}^2}{m} + v_y\omega \\ \dot{v}_y = \frac{F_Y}{m} - v_x\omega \\ \dot{\omega} = \frac{M_Z}{I_Z} \end{cases} \tag{6}$$

Where v_x and v_y are longitudinal speed and lateral speed, respectively. m is vehicle mass, I_Z is the inertia of the vehicle and C_a is the air resistance coefficient. F_X, F_Y, and M_Z are the longitudinal force, the lateral force and the yaw moment. Assuming that the front wheel yaw angle is small with other influencing factors, the they can be expressed as follows:

$$\begin{cases} F_X = F_{xrl} + F_{xrr} + \left(F_{xfl} + F_{xfr}\right)cos\delta_f \\ F_Y = F_{yfl} + +F_{yrl} + F_{yfr} + F_{yrr} \\ M_Z = l_s\left(F_{xfr} - F_{xfl}\right)cos\delta_f + l_f\left(F_{yfl} + F_{yfr}\right) + l_s(F_{xrr} - F_{xrl}) - l_r\left(F_{yrl} + F_{yrr}\right) \end{cases} \tag{7}$$

Where F_{xi} and F_{yi} are tire longitudinal and transverse forces, respectively. There is $i = fl, fr, rl, rr$. The above four corner marks represent the front left wheel, the front right wheel, the rear left wheel and the rear right wheel respectively. l_f and l_r are the distances from the center of gravity to the front and rear axles, respectively. l_s is half the width of the track and δ_f is the front wheel yaw angle.

In the controller design stage, given the strict requirements of real-time response speed and computational efficiency, it is impractical to adopt complex tire models. Thus, this study adopts a simplified linear characterization to approximate the front and rear tire lateral forces as $F_{yf} = c_f\alpha_f$ and $F_{yr} = c_f\alpha_r$ respectively, where α_f and α_r represent the side slip angles of the front and rear tires, with the specific calculation formulas as follows:

$$\alpha_f = \delta_f - \frac{\omega l_f + v_y}{v_x}, \quad \alpha_r = \frac{\omega l_r - v_y}{v_x}.$$

The following virtual control inputs are synchronously built:

$$\begin{cases} u_1 = F_{xfl}cos\delta_f + F_{xrl} \\ u_2 = F_{xfr}cos\delta_f + F_{xrr} \\ u_3 = \delta_f \end{cases} \tag{8}$$

Combining (7) with (8), the kinetic expression (6) can be expressed in the form:

$$\begin{cases} \dot{v}_x = v_y\omega + \frac{1}{m}(u_1 + u_2) - \frac{1}{m}C_a{v_x}^2 + \zeta_1 \\ \dot{v}_y = -v_x\omega + \frac{c_r l_r - c_f l_f}{m v_x}\omega - \frac{c_f + c_r}{m v_x}v_y + \frac{c_f}{m}u_3 + \zeta_2 \\ \dot{\omega} = -\frac{c_f {l_f}^2 + c_r {l_r}^2}{I_z v_x}\omega + \frac{c_r l_r - c_f l_f}{I_z v_x}v_y + \frac{c_f l_f}{I_z}u_3 + \frac{l_s}{I_z}(u_2 - u_1) + \zeta_3 \end{cases} \tag{9}$$

Where $\zeta 1$, $\zeta 2$, and $\zeta 3$e are unsimulated kinetic parameters. Furthermore, kinetic formula (9) can be expressed as:

$$\begin{cases} \dot{v}_x = v_y\omega + \frac{1}{\mathrm{m}}\ (u_1 + u_2)\ + \varepsilon_1(v_x, v_y, \omega) \\ \dot{v}_y = -v_x\omega + \frac{c_f}{m}u_3 + \varepsilon_2(v_x, v_y, \omega) \\ \dot{\omega} = \frac{c_f l_f}{I_z}u_3 + \frac{l_s}{I_z}(u_2 - u_1) + \varepsilon_3(v_x, v_y, \omega) \end{cases} \tag{10}$$

Where

$$\begin{cases} \varepsilon_1(v_{x,}v_y, \omega) = -\frac{1}{m}C_a{v_x}^2 + \zeta_1 \\ \varepsilon_2(v_x, v_y, \omega) = \frac{c_r l_r - c_f l_f}{m v_x}\omega - \frac{c_f + c_r}{m v_x}v_y + \zeta_2 \\ \varepsilon_3(v_x, v_y, \omega) = \frac{(c_r l_r - c_f l_f)v_y - (c_f {l_f}^2 + c_r {l_r}^2)\omega}{I_z v_x} + \zeta_3 \end{cases} \tag{11}$$

Where $\varepsilon_{1,2,3}(v_x, v_y, \omega)$ are the lumped uncertainty terms in the longitudinal, lateral and yaw motion of the vehicle respectively, which include three main factors: nonlinear characteristics of the tire, unmodeled dynamics of the system and external environment disturbance.

Generally, the dynamic governing equation of the vehicle system can be summarized by the following formula:

$$\dot{\boldsymbol{v}} = \boldsymbol{\psi}(\boldsymbol{v})\boldsymbol{v} + \boldsymbol{C}\boldsymbol{u} + \boldsymbol{\varepsilon} \tag{12}$$

Where $\boldsymbol{v} = [v_x, v_y, \omega]^T$ represents the velocity vector, $\boldsymbol{\varepsilon} = [\varepsilon_1(v_x, v_y, \omega), \varepsilon_2(v_x, v_y, \omega), \varepsilon_3(v_x, v_y, \omega)]^T$ denotes the lumped uncertainty vector, $\boldsymbol{u} = [u_1, u_2, u_3]^T$ denotes the virtual control input vector. $\boldsymbol{\psi}(\boldsymbol{v})$ and $\boldsymbol{C}$ are represented by matrices as follows:

$$\boldsymbol{\psi}(\boldsymbol{v}) = \begin{bmatrix} 0 & \omega & 0 \\ -\omega & 0 & 0 \\ 0 & 0 & 0 \end{bmatrix}, \ \boldsymbol{C} = \begin{bmatrix} \frac{1}{m} & \frac{1}{m} & 0 \\ 0 & 0 & \frac{c_f}{m} \\ -\frac{l_s}{I_z} & \frac{l_s}{I_z} & \frac{c_f l_f}{I_z} \end{bmatrix}. \tag{13}$$

To solve the vehicle stability control, this study proposes a novel two-step hierarchical control strategy. Compared with traditional methods, this strategy can better handle constraints and disturbances:

1. Upper layer: motion planning layer. On the premise of satisfying the constraints of longitudinal velocity and yaw rate, a feasible reference trajectory is generated to provide a target for the underlying control.

Lower layer: execution control layer. Based on the nonlinear disturbance observer, a finite-time controller is designed to generate the front wheel steering angle and virtual control force to compensate for the unmodeled dynamic characteristics and external disturbances. Through hierarchical control, the cooperative optimization control of trajectory tracking and vehicle stability is realized.

3. Controller Design

3.1 Predictive Performance Constraint Design

For the transient and steady-state performance constraints of vehicle trajectory tracking error, PPF is introduced in this study, and the core objectives of PPF are:

1. Ensure control stability: By dynamically compressing the tracking error boundary, control instability caused by factors such as actuator saturation or road disturbance can be avoided.

2. Simplify control design: Through error space mapping, the originally constrained nonlinear control problem is transformed into an easy-to-solve unconstrained optimization problem, thus simplifying the controller design process.

(1) Time-varying Performance Boundary Design

The allowable fluctuation range of tracking error $e(t)$, such as lateral position deviation y_es or yaw angle deviation φ_e is defined as:

$$\theta(t) = (\theta_0 - \theta_\infty)e^{-Kt} + \theta_\infty \tag{14}$$

Where $\theta_0 = [\theta_{0\ (1)}, \theta_{0\ (2)}, \theta_{0\ (3)}]^T$ is the upper bound of the initial allowable error. $\theta_\infty = [\theta_{\infty(1)}, \theta_{\infty(2)}, \theta_{\infty(3)}]^T$ is the upper bound of steady-state allowable error. $K = diag([K_1, K_2, K_3])$ is an exponential decay rate matrix, which controls the boundary shrinkage rate. t is time.

The corresponding lower bound is set by the scaling factor to $p \in (0,1)$:

$$\theta_{low}(t) = -p\theta(t) \tag{15}$$

(In this design, there is $p = 0.7$, the allowable lower bound is $-0.7\theta(t)$ to avoid controller conservatism caused by excessive constraints.)

(2) Error Space Mapping

To map the constrained error $e(t) \in [\theta_{low(t)}, \theta(t)]$ to the unconstrained space, the original error is first converted to the relative boundary scale:

$$\lambda = \frac{e(t)}{\theta(t)} \tag{16}$$

Furthermore, the constrained error $\lambda \in (-p, p)$ is mapped to the unconstrained space by a symmetric logarithmic function:

$$z_1 = \frac{1}{2} ln(\frac{\lambda+p}{p-\lambda}) \tag{17}$$

This transformation guarantees $e(t)$ to strictly satisfy $-p\theta(t) < e(t) < \theta(t)$, and there is $z_1 \in (-\infty, +\infty)$. Thus, it is convenient for the subsequent design of Lyapunov controller based on z_1.

3.2 Terminal Sliding Mode Controller (TSMC)

As mentioned earlier, TSMC is applied to the design of speed tracking controllers for its finite time convergence and excellent steady-state performance. Its terminal sliding surface is defined as follows:

$$\boldsymbol{s} = \dot{\boldsymbol{e}} + \gamma E \ , \ \dot{E} = sig^{\epsilon}(\dot{\boldsymbol{e}}) \tag{18}$$

Where $e = [\upsilon_{xd} - \upsilon_x, \upsilon_{yd} - \upsilon_y, \omega_d - \omega]^T$ is the error vector of the three speeds of the vehicle $\upsilon_x, \upsilon_y, \omega$. The positive design parameters is $\boldsymbol{\gamma} = diag([\gamma_1, \gamma_2, \gamma_3])$, $\boldsymbol{s} = [s_1, s_2, s_3]^T, sig^{\epsilon}(\boldsymbol{e}) = sgn(\boldsymbol{e})|\boldsymbol{e}|^{\epsilon}$. There is the parameter $\boldsymbol{\epsilon} = diag([\epsilon_1, \epsilon_2, \epsilon_3])$corresponding to $0 < \epsilon_i < 1(i = 1,2,3)$. The exponential achievement law $\dot{\boldsymbol{s}} = -\boldsymbol{\eta s} - \boldsymbol{\vartheta} sgn(\boldsymbol{s})$ is applied, where the corresponding parameters are $\boldsymbol{\eta} = diag([\eta_1, \eta_2, \eta_3])$ and $\boldsymbol{\vartheta} = diag([\vartheta_1, \vartheta_2, \vartheta_3])$. $\eta_i(i = 1,2,3)$ and $\vartheta_i(i = 1,2,3)$are the positive design parameters respectively. The system control law can be designed as follows:

$$\boldsymbol{u} = \boldsymbol{C}^{-1}(\dot{\boldsymbol{\upsilon}}_{\boldsymbol{d}} + \boldsymbol{\gamma}\dot{E} + \boldsymbol{\eta s} + \boldsymbol{\vartheta} sgn(\boldsymbol{s}) - \boldsymbol{\psi}(\boldsymbol{\upsilon})\boldsymbol{\upsilon}) \tag{19}$$

Where $\upsilon_d = \left[\upsilon_{xd}, \upsilon_{yd}, \omega_d\right]^T$ is the desired velocity vector.

Theorem 1: For system (10), when the terminal sliding surface is selected as (18) and the system control law of the controller is designed as (19), the tracking error will converge to zero in a finite time.

The Lyapunov function is selected as follows:

$$V_1 = \frac{1}{2}\boldsymbol{s}^T\boldsymbol{s} \tag{20}$$

By differentiating equation (20) with respect to the time variable, there is:

$$\begin{aligned} \dot{V}_1 = \boldsymbol{s}^T\dot{\boldsymbol{s}} &= \boldsymbol{s}^T\left(\ddot{\boldsymbol{e}} + \gamma\dot{E}\right) \\ &= \boldsymbol{s}^T\left(\ddot{\boldsymbol{\upsilon}}_{\boldsymbol{d}} - \ddot{\boldsymbol{\upsilon}} + \boldsymbol{\gamma}\dot{E}\right) \\ &= \boldsymbol{s}^T(\ddot{\boldsymbol{\upsilon}}_{\boldsymbol{d}} - (\psi(\boldsymbol{\upsilon})\dot{\boldsymbol{\upsilon}} + \boldsymbol{C}\dot{\boldsymbol{u}}) + \boldsymbol{\gamma}\dot{E}) \end{aligned} \tag{21}$$

Adding the system control law (19) to (21) leads to the following:

$$\dot{V}_1 = \boldsymbol{s}^T(-\boldsymbol{\eta s} - \boldsymbol{\vartheta} sgn(\boldsymbol{s})) \leq 0 \tag{22}$$

Theorem 1 can be proved under the framework of Lyapunov's stability theorem. Therefore, the proposed TSMC can ensure that the tracking error converges in a limited time, thus ensuring the robustness of the vehicle system.

4. Results and Discussion

4.1 Environment Settings

(1) Vehicle Parameter

Parameter	Value	Unit
m	1128.3	kg
C_a	0.4	
c_f	60000	N/rad
c_r	60000	N/rad
l_r	1.468	m

l_f	1.005	m
l_s	1.440	m
I_z	1633	$kg \cdot m^2$
h_g	0.533	m

The vehicle dynamic parameters used in this study are all extracted from the standard model in the CarSim vehicle simulation database, and the parameter selection strictly follows the recommended range of the database to ensure consistency with the dynamic characteristics of typical passenger cars, thus avoiding the error caused by subjective assumptions.

(2) Simulation Parameters of Control System

Design Parameters
$K_1 = K_2 = K_3 = 4$
$\gamma_1 = \gamma_2 = \gamma_3 = 15.5$
$\epsilon_1 = \epsilon_2 = \epsilon_3 = 0.5$
$\eta_1 = 2,\ \eta_2 = 1,\ \eta_3 = 2$
$\vartheta_1 = 1,\ \vartheta_2 = 2,\ \vartheta_3 = 4$

(3) Environmental Assumptions

Pavement conditions: This experiment takes standard dry asphalt pavement as the test benchmark, which does not include the influence of extremely low adhesion coefficient working conditions to simplify the model assumptions and ensure the stability of the results.

External disturbance: It is assumed that there is no persistent crosswind interference during the experiment, and the small impact of environmental noise on sensor data is ignored, aiming to highlight the performance of the system itself.

4.2 Simulink Simulation Results

After Simulink simulation and error constraint design based on the prediction performance function, the response of longitudinal speed error, lateral speed error and yaw rate error of the system with time are shown in Figure 2 to Figure 6 respectively.

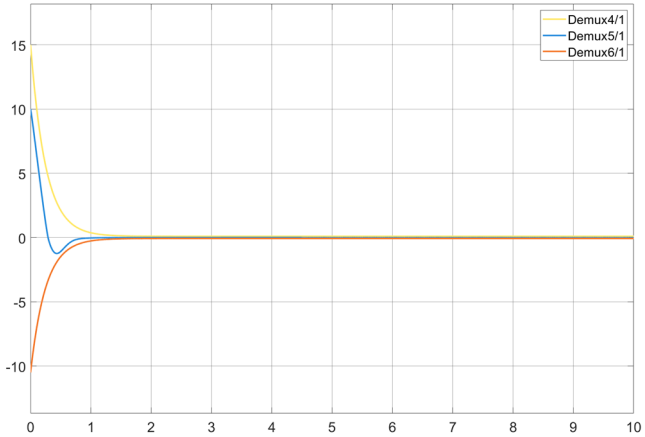

Figure 2 Response Curve of Error v_x

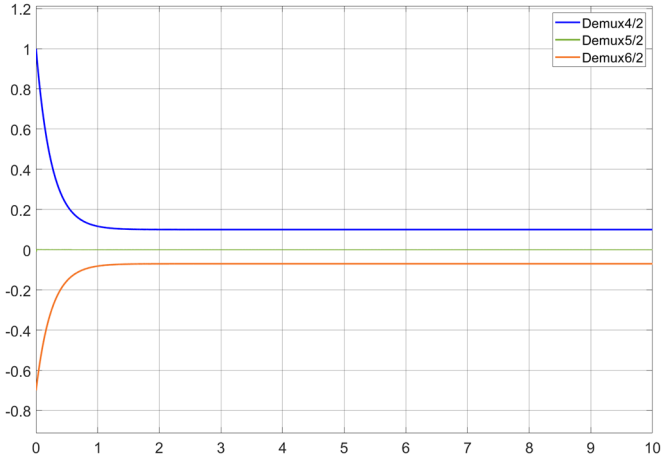

Figure 3 Response Curve of v_y

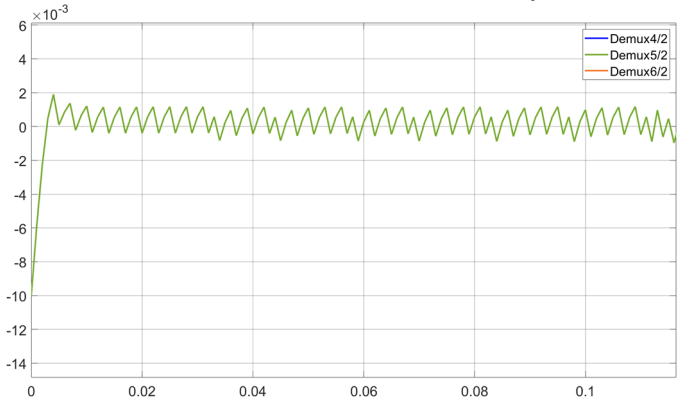

Figure 4 Initial Response of Error v_y

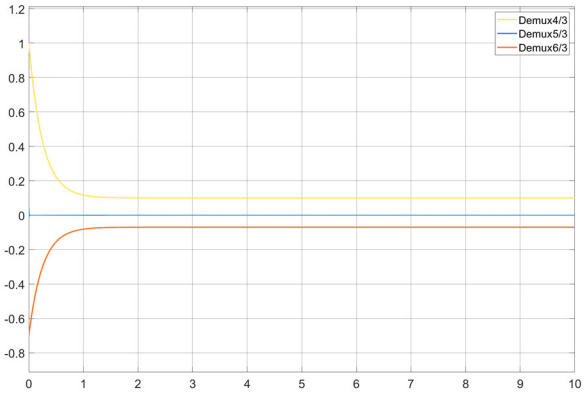

Figure 5 Response Curve of Error ω

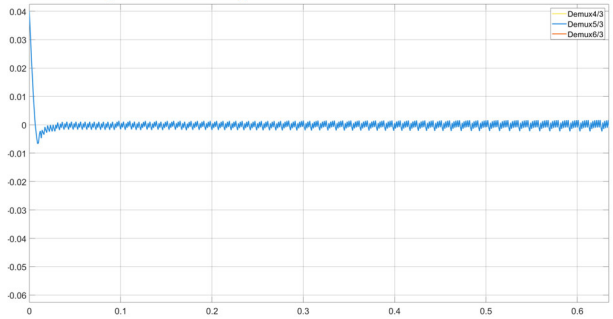

Figure 6 Initial Response of Error ω

According to Figure 2, the longitudinal velocity error approaches the preset upper limit of the performance boundary at the beginning of the simulation. With the progress of time, the dynamic

adjustment mechanism based on the PPF makes the error amplitude gradually attenuate, which finally stabilizes in an apparently narrowed constraint interval. PPF effectively reduces the initial control input requirement of the system by setting an initial wide performance boundary. With the gradual tightening of the boundary, the steady-state error is further suppressed, which fully reflects the adaptive matching ability of the dynamic characteristics of the system.

Figure 3 and Figure 4 indicate that the lateral velocity error fluctuates slightly throughout the simulation and is always strictly constrained within the preset performance boundary range. The error curve shows no obvious trend close to the upper and lower bounds, which indicates that PPF can actively adjust the error boundary by predicting the lateral dynamic state of the vehicle in real time, and suppressing the potential disturbance on the system performance.

Based on Figure 5 and Figure 6, the yaw rate error keeps low amplitude oscillation during the whole simulation without transient fluctuation close to the boundary, which verifies the synergistic effect of the TSMC and the PPF boundary prediction function. The control strategy directly suppresses the accumulation of heading error from the control law design, which proves good robustness and error constraint ability.

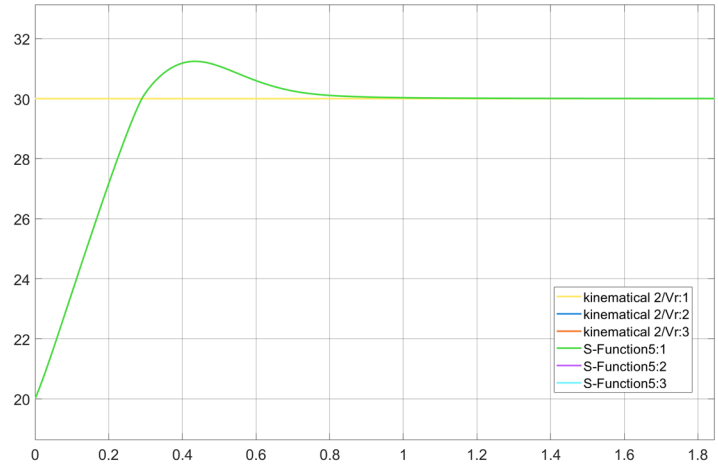

Figure 7 Tracking Comparison of v_x

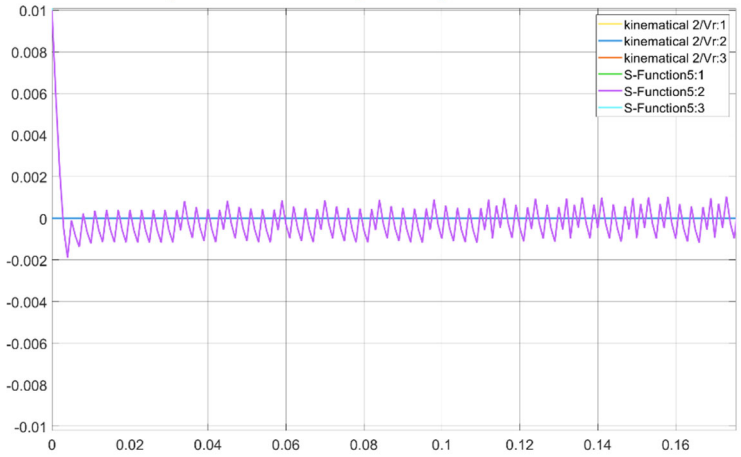

Figure 8 Tracking Comparison of v_y

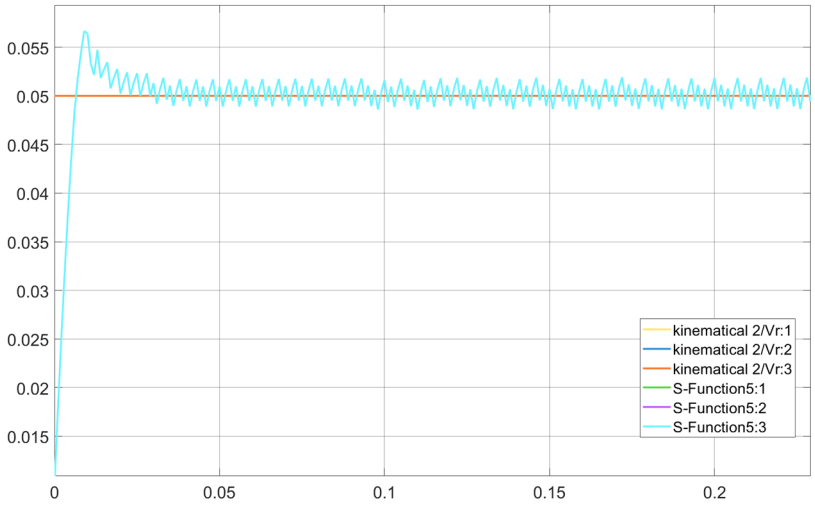

Figure 9 Tracking Comparison of ω

Figures 7 to 9 indicate the tracking comparison of longitudinal speed, lateral speed and yaw rate, fully revealing the comprehensive control efficiency based on the collaborative architecture of PPF and TSMC. The progressive convergence of longitudinal velocity in the figure fully reflects the dynamic compensation of the controller for the inertial characteristics of the system, and suppresses the overshoot and oscillation in the initial stage. The lateral velocity and yaw velocity only show slight fluctuations, which verifies the robustness and accuracy of the cooperative constraint of multi-degree-of-freedom state variables.

It is worth noting that the response of the yaw rate shows significantly improved smoothness compared with the traditional sliding mode control scheme, thanks to the elastic boundary designed by PPF that provides an effective chattering suppression space for TSMC and reduces the frequent switching of control inputs. Meanwhile, the high time series consistency between the predicted trajectory and the actual control output shows that the close cooperation between the rolling optimization algorithm and the real-time control strategy overcomes the dynamic lag between the model and the actual vehicle dynamics, which improves the tracking accuracy and the overall robustness of the system.

5. Conclusion

Aiming at the challenge of coupling dynamic uncertainty and multi-degree-of-freedom in vehicle trajectory tracking control, a composite control architecture based on PPF and TSMC is proposed in this study. The deep fusion of time-varying performance boundary and finite-time convergence of terminal sliding mode is realized for the first time. PPF constructs an elastic performance funnel through the evolution trend of dynamic prediction error, which provides an adaptive feasible domain for sliding mode control. Based on the feasible region, TSMC designs the terminal attractor, which realizes the fast convergence of tracking error and chattering suppression. Their organic synergy effectively breaks the inherent contradiction between tracking accuracy and robustness in traditional control methods, which opens up a new paradigm for efficient tracking control of complex dynamic systems.

References

[1] K. D. Young and Ü. Özgüner, "Sliding mode control with perturbation estimation," IEEE Trans. Control Syst. Technol., vol. 7, no. 3, pp. 328-338, May 1999.

[2] D. Q. Mayne, J. B. Rawlings, C. V. Rao, and P. O. M. Scokaert, "Constrained model predictive control: Stability and optimality," Automatica, vol. 36, no. 6, pp. 789-814, Jun. 2000.

[3] M. Van, S. S. Ge, and H. L. Ren, "Finite time fault tolerant control for robot manipulators using time delay estimation and continuous nonsingular fast terminal sliding mode control," IEEE Trans. Cybern., vol. 47, no. 7, pp. 1681-1693, Jul. 2016.

[4] H. H. Pan, W. C. Sun, H. J. Gao, and J. Y. Yu, "Finite-time stabilization for vehicle active suspension systems with hard constraints," IEEE Trans. Intell. Transp. Syst., vol. 16, no. 5, pp. 2663-2672, Oct. 2015.

[5] Q. L. Hu and X. D. Shao, "Smooth finite-time fault-tolerant attitude tracking control for rigid spacecraft," Aerospace Sci. Technol, vol. 55, pp. 144-157, 2016.

[6] M. Chen, Q. X. Wu, and R. X. Cui, "Terminal sliding mode tracking control for a class of SISO uncertain nonlinear systems," ISA Trans., vol. 52, no. 2, pp. 198-206, Mar. 2013.

[7] M. Yue, L. J. Wang, and T. Ma, "Neural network-based terminal sliding mode control for WMRs affected by an augmented ground friction with slippage effect," IEEE/CAA J. Autom. Sin., vol. 4, no. 3, pp. 498-506, Jul. 2017.

[8] Q. L. Hu and B. Y. Jiang, "Continuous finite-time attitude control for rigid spacecraft based on angular velocity observer," IEEE Trans. Aerosp. Electron. Syst., vol. 54, no. 3, pp. 1082-1092, Jun. 2018.

[9] C. P. Bechlioulis and I. S. Rovithas, "Robust adaptive control of nonlinear systems with prescribed transient performance," IEEE Trans. Autom. Control, vol. 53, no. 9, pp. 2090-2099, Oct. 2008.

[10] T. P. Brekaki, A. A. Kaskanis, and I. S. Rovithas, "Prescribed performance control," Annu. Rev. Control, vol. 53, pp. 327-340, 2022.

[11] S. Li, L. Shi, W. Zhang, and H. Gao, "Performance prediction-based adaptive iterative learning control for batch processes with time-varying uncertainties," J. Process Control, vol. 90, pp. 94-105, 2020.